Blackbody-induced radiative dissociation of cationic SF_6 clusters

Y. Toker,[1,*] I. Rahinov,[1,†] D. Schwalm,[1,‡] U. Even,[2] O. Heber,[1] M. L. Rappaport,[1] D. Strasser,[3] and D. Zajfman[1]

[1]*Department of Particle Physics and Astrophysics, Weizmann Institute of Science, Rehovot 76100, Israel*

[2]*Raymond and Beverly Sackler School of Chemistry, Tel-Aviv University, Tel Aviv 69978, Israel*

[3]*Institute of Chemistry, Hebrew University, Jerusalem 91904, Israel*

(Received 4 July 2012; published 20 August 2012)

The stability of cationic $SF_5^+(SF_6)_{n-1}$ clusters was investigated by measuring their blackbody-induced radiative dissociation (BIRD) rates. The clusters were produced in a supersonic expansion ion source and stored in an electrostatic ion-beam trap at room temperature, where their abundances and lifetimes were measured. Using the "master equation" approach, relative binding energies of an SF_6 unit in the clusters could be extracted from the storage-time dependence of the survival probabilities. The results allow for a deeper insight into the effect of a localized charge on the structure and stability of SF_6-based clusters.

DOI: 10.1103/PhysRevA.86.023202 PACS number(s): 36.40.Mr, 36.40.Qv, 36.40.Wa

I. INTRODUCTION

What is the effect of a charge on the structure and stability of clusters? If a positive charge is localized on one cluster unit (an atom or a molecule), one would expect that the lowest energy configuration of the cluster is that of the ion as a central core and neutral units forming shells around it, since the monopole induced-dipole force between the ion and neutral units is stronger than the dipole-dipole forces between the neutral units. One would also expect that the resulting clusters are more stable than their neutral counterparts. However, this simple picture is not generally valid. For metal clusters, the charge is found to be delocalized over the whole cluster [1], and, e.g., for noble gas clusters it is conjectured that the charge is delocalized over several atoms, forming a linear ionic molecule which then serves as an ionic core, leading to cigar-shaped clusters [2]. In molecular clusters, on the other hand, the charge is often localized on an atomic or molecular core, but here the internal structure of the molecules may lead to considerably more complex structures, a typical example being charged water clusters, which have received a great deal of attention due to their importance for chemistry and biology [3]. The present work is focused on a conceptually simpler molecular system, that of the SF_6 molecule which—due to its highly symmetric octahedral shape—is often thought of as semispherical or a "big noble gas atom". However, due to the stability of the SF_6 molecule, one does not expect charge delocalization in cationic sulfurhexafluoride clusters involving SF_a^+ ($a = 3,4,5$) as a charge carrier.

A procedure often applied to deduce information about the stability of clusters is to determine their abundance in beams emerging from a cluster-ion source via time-of-flight techniques. The measured cluster abundances are usually not smooth functions of their size but show intriguing structures where individual clusters are produced much more abundantly than others, a phenomena sometimes referred to as "magic numbers" [4]. These structures are commonly interpreted in terms of stability—the more stable a cluster is the more abundantly will it be produced—and the stability in turn is interpreted in terms of cluster structures. Cluster abundance measurements have led to many important fundamental discoveries such as electronic shell closing [1], the Buckminster fullerene [5], icosahedral shell closing [6], and geometrical shell closing in general [7]. However, inferring the stability of clusters from their mass spectra is in most cases done only qualitatively, since the process of cluster formation in a cluster-ion source is extremely complex. This is thought to be true, in particular, for cationic SF_6 clusters (see, e.g., Ref. [8]), as electron impact methods used to produce these clusters result in the ejection of at least one F atom from one of the SF_6 units, which might lead to extensive fragmentation. Depending on whether the ionization occurs in an early or late phase of the aggregation, this might have quite a different effect on the abundance pattern.

For a more quantitative understanding of cationic clusters, one would therefore like to measure directly the stability of the cluster against fragmentation, i.e., the binding energy E_0 of a cluster unit in the cluster. One tool for doing this is blackbody-induced radiative dissociation (BIRD) [9]. BIRD occurs when ions are stored in high vacuum within a trap whose temperature is equal to or higher than the temperature required for the ions to dissociate. As the ions are stored, they heat up by absorbing infrared (IR) photons from the ambient radiation field until they eventually fragment. By measuring the rate at which the clusters dissociate one can extract the barrier (activation) energy E_b, which will be equal to the binding energy E_0 in case the dissociation process does not have a reverse activation barrier. The BIRD process has been used to study the stability of organic molecules [9], and it has also been applied to water-based clusters of the form $X^+(H_2O)_n$, exemplifying the use of the method for cluster research [3].

In this work the BIRD-induced decays of cationic $SF_5^+(SF_6)_{n-1}$ clusters are measured in a setup which combines an Even-Lavie supersonic expansion ion source [10] with an electrostatic ion-beam trap (EIBT) [11] at room temperature. The time dependence of the survival probability of the cluster will be discussed on several levels of sophistication in the

*Present address: Institute of Physics and Astronomy, University of Aarhus, DK-8000 Aarhus C, Denmark.

†Present address: Department of Natural Sciences, The Open University of Israel, Raanana, 43107, Israel.

‡Permanent address: Max-Planck-Institut für Kernphysik, D-69117 Heidelberg, Germany.

analysis. It will be shown that the survival probability averaged over approximately 80 ms, and the BIRD rate extracted in a crude analysis reveals major trends such as the closing of geometric shells and subshells, essentially independent of the cluster formation process. Moreover, we will show that relative binding energies can be extracted from the time dependence of the survival curves using a "master equation" approach, which allows for a deeper insight into the relation between abundance and stability and into the structure of cationic SF_6 clusters.

A. SF_6-based clusters

The SF_6 molecule consists of a central sulfur atom surrounded by six fluorine atoms positioned on the vertices of an octahedron. The molecule, which is in gas phase at room temperature, is extremely inert and therefore often considered as a big noble gas atom. However, unlike atoms, the molecule is a remarkably efficient absorber of IR radiation, exhibiting a very strong IR absorption band at 10.6 μm and a second, approximately 10 times weaker band at 16 μm [12]. The relative simplicity of the SF_6 structure and its strong IR absorption make SF_6-based clusters interesting candidates for BIRD studies. A further advantage of SF_6-based clusters as a model system is the availability of detailed knowledge of the bulk properties of solid and liquid SF_6, information that facilitates modeling of the BIRD process.

The structure of $(SF_6)_n$ clusters produced in supersonic expansion sources has been studied by electron-attachment time-of-flight mass spectrometry [8,13], by electron diffraction [14], and by calculations [15,16]. These studies indicate that small clusters assume icosahedral structures, while large clusters have a bcc structure. Indeed, measured relative abundances display a pronounced maximum at $n = 13$, which is attributed to the closing of the first icosahedral shell. If the icosahedral structure would persist for larger clusters, one would expect the next magic number associated with the closing of the second icosahedral shell to be $n = 55$. However, for $n = 55$ the abundance spectrum actually displays a minimum. Instead, the next magic number is observed at $n = 59$, which is attributed to a nearly spherical aggregate packed in bulk monoclinic bcc structure [8,13]. The fine structure of the abundance pattern between the two magic numbers suggests that the transition from icosahedral-based structures to bcc-like structures (known as the "cluster-to-bulk transition") seems to occur at around $n \approx 50$, which is surprising since for noble gas clusters this transition occurs at much larger sizes ($n > 1000$).

As SF_6 is a strong electron absorber, SF_6^- ions as well as $(SF_6)_n^-$ clusters are readily produced by electron attachment in supersonic expansion ion sources. And, as electron attachment is believed to be a very gentle process, abundance measurements performed with anionic $(SF_6)_n^-$ clusters are therefore considered to reflect the abundance and structure of neutral $(SF_6)_n$. Experiments have failed, on the other hand, to produce the positive SF_6^+ ion or positive $(SF_6)_n^+$ clusters; the removal of an electron from SF_6 is always accompanied by the loss of at least one F atom. Consequently, upon ionization, cluster series of the form $SF_a^+(SF_6)_{n-1}$ (with $a = 3,4$, and 5) are created in supersonic expansion ion sources. Mass spectrometric studies of these cationic SF_6 clusters by time-of-flight techniques have been conducted in the 1980s [17,18]. For the $SF_5^+(SF_6)_{n-1}$ series, these studies reached up to $n \approx 40$; they resulted in relative abundances which indicate that $n = 13$ is a magic number also for cationic SF_6 clusters, while an abundance dip was observed at $n = 18$.

To the best of our knowledge, the only attempt so far to measure binding energies of SF_6-based clusters has been performed by Hiraoka *et al.* [19], who measured the stability of the cluster ions $SF_a^+(SF_6)_{n-1}$ with $a = 0-5$ and $n = 2-4$ using a high-pressure mass spectrometer. They concluded that the interaction between SF_5^+ and SF_6 is exceptionally weak compared to the other SF_a^+ ions and determined the corresponding reaction enthalpies at standard conditions for $SF_5^+(SF_6)_{n-1} \rightarrow SF_5^+(SF_6)_{n-2} + SF_6$ with $n = 2$ and 3 to be 202 and 155 meV, respectively. For neutral $(SF_6)_n$ clusters, calculated binding energies are available for $n = 2$ to $n = 10$ [16]. These binding energies show an increase from $E_0 = 67$ meV for the dimer to 118 and 155 meV for the trimer and tetramer, and up to 202 meV for $n = 10$, where they seem to level off towards the bulk value of ~230 meV expected according to the molar sublimation enthalpy measured at $T = 186$ K [20]. In view of the calculated binding energies for $(SF_6)_n$, the smallness of the molar enthalpy measured for $SF_5^+(SF_6)_{n-1} \rightarrow SF_5^+(SF_6)_{n-2} + SF_6$ is surprising. Taken at face value it means that the binding energy of SF_6 in $SF_5^+(SF_6)_2$ is only as large as in $(SF_6)_4$, i.e., the effect of the polarizing charge on the binding of an SF_6 unit is already lost for $n \gtrsim 3$. Intuitively, one would not expect this to take place before the closing of the first icosahedral shell at $n = 13$.

B. BIRD–Blackbody-induced radiative dissociation

When molecules or clusters are stored under ultrahigh vacuum conditions, they do not equilibrate with the environment through collisions with residual gas molecules; however, they do interact with the surrounding by the absorption and emission of IR photons. For cold cluster ions stored in a trap at temperature T_{trap} the interaction with the IR radiation will heat up the clusters until they eventually thermalize to the trap temperature. However, for loosely bound molecules or clusters with low barrier energies E_b for dissociation, the heating might cause the ions to fragment. This process is known as blackbody-induced radiative dissociation (BIRD) [9], and the rate at which ions dissociate due to this process is known as the BIRD rate. Thus BIRD is a multistep process including first the absorption of IR radiation and then statistical dissociation.

It was first realized by the Williams group [21] that in the limit where statistical dissociation is much slower than IR absorption, the ions will first quickly equilibrate to the temperature of the trap and then slowly dissociate. Thus the statistical dissociation rate is the dominant factor determining the BIRD rate, in which case it is given by the Arrhenius law

$$k = Ae^{-\frac{E_b}{k_B T_{\text{trap}}}}, \tag{1}$$

where A is called the frequency or Arrhenius parameter and k_B is the Boltzmann constant. Therefore, by measuring k as a function of the trap temperature T_{trap} the barrier energy E_b can be extracted. This limit is known as the "rapid exchange" limit and is found to be fulfilled, e.g., by biomolecules and large molecular clusters.

In the other limit, in which the dissociation rate is getting faster than the IR absorption rate during the warming of the clusters, the ions will fragment before thermal equilibrium with the trap temperature is reached. In this case, which may be referred to as the "slow exchange" or as the "sudden death" limit [9], extraction of the barrier energy is not as straightforward as in the rapid exchange limit. In the slow exchange limit the decay of the ions is not expected to be exponential because it is a result of a multistep process involving the absorption of enough IR photons to cross the barrier for fragmentation. One has also to account for the initial energy distribution of the clusters. Thus the hottest members of the ensemble might not require IR absorption for dissociation and will decay at very early times. Nevertheless, the experimental data and the modeling presented in this work show that for long storage times the decay does become approximately exponential. This suggests that after a certain elapsed time t_e, the clusters reach a kind of dynamic equilibrium. We will refer to the approximately constant rate of decay reached for $t > t_e$ as the BIRD decay rate k_{BIRD}.

The slow exchange limit implies that the process of IR absorption is the limiting factor for the BIRD decay rate. For molecular clusters containing n IR-active molecules such as the SF_6-based clusters investigated in the present study, the energy intake will be dominated by transitions within the individual molecules. Assuming the (average) IR absorption rate of a single molecule to be k_{IR} and that the absorbed energy $\hbar\omega$ is immediately dumped into the cluster degrees of freedom such that spontaneous and induced IR emission can be neglected, we can expect k_{BIRD} to be approximately proportional to k_{IR} and to scale linearly with the number of IR-active molecules in the cluster, that is,

$$k_{\mathrm{BIRD}} = n k_{\mathrm{IR}} F(E_b, T_i, \hbar\omega, \Delta t, \ldots) \qquad (2)$$

for storage times $t \gtrsim t_e$. The function F contains the dependence of k_{BIRD} on the barrier energy E_b, the initial conditions such as the initial cluster temperature T_i, and on the energy $\hbar\omega$ of the absorbed IR photons as well as the storage-time interval Δt. A nice example for the validity of Eq. (2) has been observed when studying the infrared-induced fragmentation of water clusters [3], which exhibit an overall linear dependence of the BIRD rates on the number of water molecules in the cluster, with less stable clusters than the average being reflected by higher BIRD dissociation rates and vice versa.

As will be discussed below, the decay rates measured for the cationic $SF_5{}^+(SF_6)_{n-1}$ clusters stored in a room-temperature trap exhibit a behavior very similar to that of the water clusters discussed in Ref. [3]. It will be shown that Eq. (2) can be used for a qualitative analysis of the decay curves. Nevertheless, a more complete understanding of the decay characteristics of the clusters in terms of the barrier energies E_b can only be achieved by detailed modeling of the BIRD process, which also takes into account the initial nonexponential decay.

II. EXPERIMENTAL SETUP

The experimental setup used in this work is illustrated schematically in Fig. 1. It consists of an "Even-Lavie" supersonic expansion ion source [10] that is coupled to an electrostatic ion beam trap (EIBT) [11]. In the supersonic expansion ion source, a gas mixture of 1% SF_6 in neon at a total pressure of 24 bar supersonically expands through a pulsed nozzle (pulse duration 20 μs) into the vacuum system. As the expansion proceeds, the temperature of the gas decreases and cluster formation begins. At a distance of 3 mm from the nozzle, the gas jet is bombarded with 200-eV electrons using a pulsed ionizer that is synchronized with the nozzle. As the electron impact occurs within the Mach zone, the formation of ionic clusters and their cooling by collisions with the carrier gas continues after the ionization. This part of the setup is mounted on a high-voltage platform. After the ions exit the platform through the skimmer they are accelerated to a kinetic energy of 4.2 keV. The time of flight of the cluster from the ionization zone to the acceleration gap is approximately $t_a \sim 180\,\mu$s.

After acceleration the ions are steered and focused by an Einzel lens and a pair of deflectors. The ion beam is then passed through a chicane beam cleaner, in which it is deflected downwards and then upwards again, while neutral particles and photons are blocked. Finally the beam is injected into the EIBT [11], which consists of two electrostatic mirrors between which the ion beam oscillates. Ions are injected into the trap by lowering the voltage on one of the electrodes (labeled as V_P in Fig. 1) of the entrance mirror and then rapidly raising it before

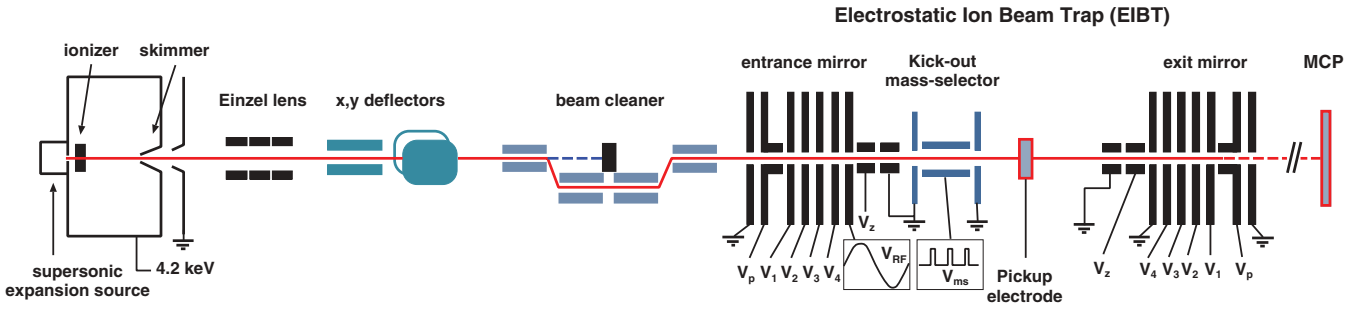

FIG. 1. (Color online) A sketch of the experimental setup. Ions are produced in a pulsed supersonic expansion ion source and accelerated to 4.2 kV. They are focused and steered by an Einzel lens and deflectors and passed through a beam cleaner before they are finally injected into the electrostatic ion-beam trap. The trap uses two electrostatic mirrors between which the ions oscillate. A pickup electrode serves to measure the charge of the oscillating ion bunches as a function of the storage time. If required, the kick-out mass selector can be employed to select from the stored ion bunch clusters of a single mass. A microchannel plate (MCP) detector, mounted downstream from the exit mirror, can be used to measure neutral fragments from ions dissociating within the trap.

the ions reflected at the exit mirror can leave the trap. During the experiments described here the residual gas pressure in the trap was around 5×10^{-10} Torr.

Located close to the center of the trap is a pickup electrode. When a bunch of ions is passing through this electrode—twice during every oscillation in the trap—their image charge is measured and recorded by a digital oscilloscope. Since the oscillation frequency of the ions f is inversely proportional to the square root of their mass $f \propto \frac{1}{\sqrt{m}}$, by Fourier transforming the pickup signal measured for some storage-time interval Δt the ion mass and the number of stored ions can be determined [11]. For a clear Fourier signal it is important that the ions remain as a bunch throughout the measurement. One elegant way of achieving this is by operating the trap in the "self-bunching" mode [22,23], where the ion bunches are held together by an interplay between Coulomb interaction and the electrostatic mirror potential. This operation mode allows for an easy and accurate assessment of the mass composition of the stored ions. A full mass spectrum can be obtained by scanning the opening time of the trap to compensate for the mass dependence of the time of flight between ion production and trap, which allows trapping of ions only within a certain mass window per injection. We shall refer to this technique as the *pickup mass spectrometry* method.

Figure 2 shows a portion of the pickup mass spectrum recorded for cationic SF_6 clusters by averaging over the first $\Delta t = 80$ ms of storage. As mentioned, upon ionization the SF_6 molecule fragments, producing predominantly SF_5^+ (∼70%), but also SF_4^+ (∼2%) and SF_3^+ ions (∼28%), which leads to three families of cationic clusters, $SF_a^+(SF_6)_{n-1}$ with $a = 3,4,5$. The shoulders visible on the high-mass side of the main peaks (see inset in Fig. 2) are due to the sulfur isotope ^{34}S, which occurs in natural sulfur with an abundance of 4.2% and which is replacing the main isotope ^{32}S in some of the SF_6 units. Additional series seen in the mass spectra correspond to the addition of one or two water molecules to the SF_6-based cluster, producing $SF_a^+(SF_6)_{n-1}(H_2O)_b$ with $b = 1,2$. In this work only the properties of the main series of $SF_5^+(SF_6)_{n-1}$ are investigated (shown as the red continuous line in Fig. 2).

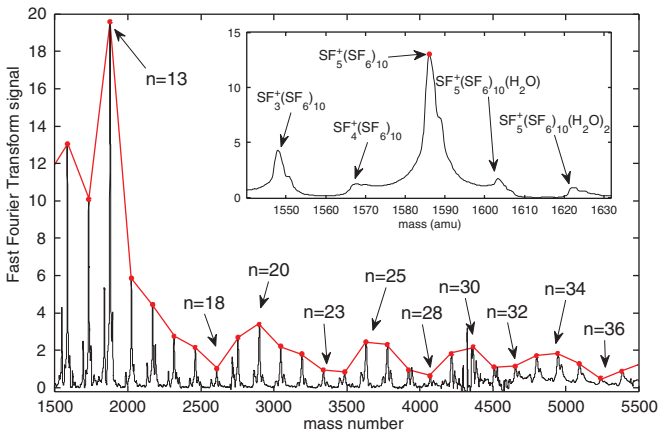

FIG. 2. (Color online) Mass spectrum of cationic SF_6 clusters obtained with the pickup mass spectrometry technique. The main series of $SF_5^+(SF_6)_{n-1}$ is emphasized by a continuous (red) envelope. The inset of the figure shows a zoom around $n = 11$.

In contrast to usual abundance measurements with time-of-flight techniques, which involve flight times of several 100 μs at most, the pickup mass spectra are obtained by averaging over a time interval comparable to the lifetimes of the cluster in the trap. As these lifetimes are dominated in the present study by the BIRD-induced dissociation rates, the intensities of the mass peaks are not only determined by the original abundance of the cluster but also by $\tau_{\mathrm{BIRD}} = 1/k_{\mathrm{BIRD}}$, which results in a considerably more pronounced intensity pattern.

As the abundances and lifetimes of the $SF_5^+(SF_6)_{n-1}$ clusters are generally decreasing for $n > 13$, it is progressively more difficult to observe the ions via their induced image charges. For clusters with $40 < n < 100$ we therefore employed a different method. This method uses the "kick-out mass selector" which is mounted between the entrance mirror and the pickup electrode (see Fig. 1) and described in more detail in Ref. [24]. A pulsed voltage train, denoted by V_{ms} in Fig. 1, is applied for the first ≈5 ms of a trapping cycle to the deflector plates of the kick-out mass selector to clear the trap of all ions but those of the desired mass m. The duration of the mass-selection pulse train was set to assure a mass resolution of $\delta m = 5$ amu. After this cleaning stage neutral fragments from disintegrating clusters are recorded as a function of storage time using the microchannel plate (MCP) detector mounted after the exit mirror of the EIBT. Relative cluster intensities were then obtained by integrating the decay curves measured for different settings of the mass selector. As the SF_6 fragments from BIRD-induced dissociation of large clusters have an energy too low to trigger the MCP, the MCP mainly detects heavy neutral fragments resulting from residual gas collisions, which are governed by a decay probability $k_{\mathrm{eff}} \ll k_{\mathrm{BIRD}}$ and which can be expected to be independent, or at least a smooth function, of n. Thus the integration over the measured decay curves leads as before to an intensity pattern which is enhanced by the BIRD effect. We shall refer to this technique as the *kick-out mass spectrometry* method.

For very light clusters, lifetime measurements can in principle be performed by monitoring the counts produced on the MCP as a function of time. For heavier clusters, however, evaporation of one cluster unit can lead to a fragment ion which is still stored within the EIBT. Therefore, in order to measure the BIRD rates of the $SF_5^+(SF_6)_{n-1}$ clusters, a mass-selective technique was employed, which we will refer to as the RF pickup method [25]. The technique relies on operating the EIBT in a normal (dispersive) mode and bunching the desired mass using a small oscillating voltage (peak-to-peak amplitude $V_{\mathrm{RF}} = 2.3$ V), which is applied to one of the electrodes in the entrance mirror (see Fig. 1) and oscillates with the same or an integer multiple of the oscillation frequency of the ions to be measured. By analyzing the charge induced by the ion bunch on the pickup electrode using a windowed fast-Fourier transform ($\Delta t = 5$ ms) one can follow the number of stored ions of the selected mass m_0 as a function of the trapping time t. It should be noted that if a cluster dissociates by emitting a neutral molecule, the remaining charged fragment has the same velocity but a smaller energy than the parent. As this leads to an oscillation frequency different from that of the parent, the daughter ion no longer contributes to the frequency signal produced by the parent ions. The RF pickup technique, which has the additional advantages of being fast

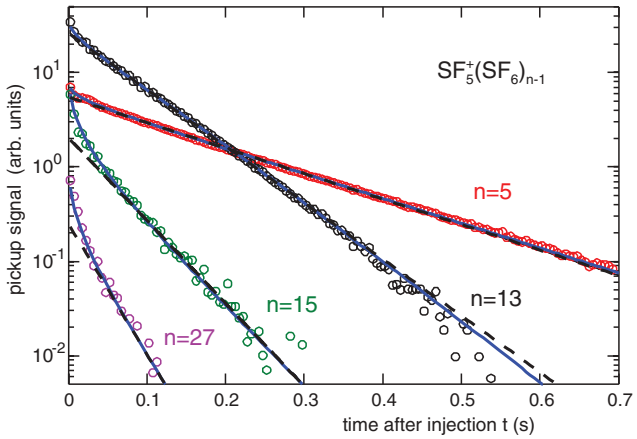

FIG. 3. (Color online) Decay curves of $SF_5{}^+(SF_6)_{n-1}$ clusters with $n = 5,13,15,27$, measured using the RF pickup technique [25]. The solid (blue) lines are fits to the data using the model described in Sec. III B. The dashed lines represent the slow components of a biexponential fit [see Eq. (3)] from which the BIRD decay rates k_{BIRD} are deduced.

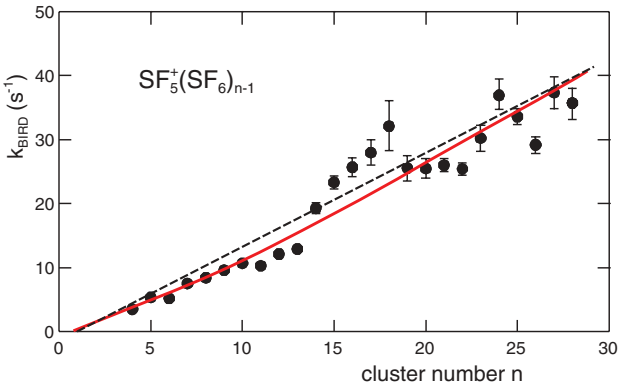

FIG. 4. (Color online) BIRD rates k_{BIRD} deduced from a biexponential fit of the measured decay curves of $SF_5{}^+(SF_6)_{n-1}$ clusters with $4 \leqslant n \leqslant 28$, which were stored in the EIBT at room temperature (error bars are reflecting statistical and fitting errors). The dashed (black) line is a fit linear in $(n-1)$ to the data, while the red (solid) line represents the BIRD rates calculated within the model discussed in Sec. III B, assuming a constant barrier energy of $E_b = 275$ meV and a constant initial cluster temperature of $T_i = 140$ K.

and not requiring mass selection prior to the measurement, was recently investigated in detail using the present experimental setup [25]. Examples of survival curves $N(t)$ measured with this technique for $SF_5{}^+(SF_6)_{n-1}$ clusters with $n = 5,13,15,27$ are shown in Fig. 3.

The BIRD process is the dominant, but not the only, loss mechanism of the $SF_5{}^+(SF_6)_{n-1}$ clusters from the trap. Other losses within the time scale of interest in the present investigations (<1 s) are due to residual gas collisions and losses inherent to the RF pickup technique. The contribution k_{rg} of residual gas collisions to the total decay rate was measured by performing lifetime measurements for some $SF_5{}^+(SF_6)_{n-1}$ clusters at different residual gas pressures between 5×10^{-10} and 3×10^{-8} Torr. For example, for $n = 13$ the residual gas-induced contribution to the total decay rate was determined to be $k_{rg} = 0.6(1)\ \mathrm{s}^{-1}$ at a residual gas pressure of $p \sim 5 \times 10^{-10}$ Torr, the pressure at which all BIRD measurements were performed. Particle losses due to the RF voltage applied to one of the electrodes of the mirrors have been investigated in detail in Ref. [25] for $SF_5{}^+$ ions and storage times $t \gtrsim 20$ ms; they were found to result in an additional decay rate of $k_{rf} = 0.8(2)\ \mathrm{s}^{-1}$ at the RF voltage applied. These RF-induced losses are expected to be proportional to the the oscillation frequency and thus proportional to $1/\sqrt{m}$. As more recent investigations [26] suggest that the RF-induced losses might be larger at storage times $t < 20$ ms, we will not consider the first three data points of the decay curves in the detailed analysis performed in Sec. III C.

III. DATA ANALYSIS AND RESULTS

A. BIRD decay rates

Figure 3 shows typical examples of decay curves measured for $SF_5{}^+(SF_6)_{n-1}$ clusters using the RF pickup technique. On long times scales ($t > 50$ ms) the decay appears to be close to exponential. The decay curves can in fact be reasonably well described by two exponentials characterized by a fast (k_f) and a slow (k_s) decay constant:

$$N(t) = N_{0,f} \exp^{-k_f t} + N_{0,s} \exp^{-k_s t}. \qquad (3)$$

While the fast decay constants derived from the biexponential fit of the data depend only moderately on the cluster number n ($k_f \approx$100–200 Hz), the slow decay constants are observed to increase approximately linearly with $n-1$, as expected according to Eq. (2) for BIRD-induced decays in the slow exchange limit. We therefore identify the slow decay constant k_s, after correcting for contributions caused by residual gas collisions and by RF bunching, with the BIRD rate k_{BIRD}. The fast decay at short storage times is due to the dissociation of hot clusters before the BIRD process starts to dominate, as will be shown in Sec. III B.

Figure 4 displays the deduced BIRD rates for $SF_5{}^+(SF_6)_{n-1}$ clusters with $4 \leqslant n \leqslant 28$ at a trap temperature of 297 K. The dashed line results from a linear fit to the data assuming $k_{\mathrm{BIRD}} \propto (n-1)$, as expected from Eq. (2) when making the (not stringent) assumption that the charged $SF_5{}^+$ unit is not contributing to the warming up of the cluster, and assuming $F(E_b, T_i, \ldots)$ to be a constant. While the overall increase of k_{BIRD} with increasing cluster number is well reproduced, pronounced deviations of the data from the straight line are observed. These deviations anticorrelate with the intensities of the $SF_5{}^+(SF_6)_{n-1}$ clusters in the mass spectrum displayed in Fig. 2 and will be shown to be useful to the understanding of the clusters' stability.

To shed some light on the heating mechanism of the clusters, we also measured the BIRD rates for $n = 13$ and $n = 14$ at elevated trap temperatures. Using the heating blankets normally employed for outgassing the trap setup, we could raise the trap temperature from $T_{\mathrm{trap}} = 297$ K by about 50 K without spoiling the trap vacuum by more than a factor of two. While a similar increase of the trap pressure by a factor of two *without* increasing T_{trap} leads to a change of the slow decay constant k_s by only ∼+4%, the temperature change by 50 K results in an increase of k_s by ∼100%. The resulting BIRD

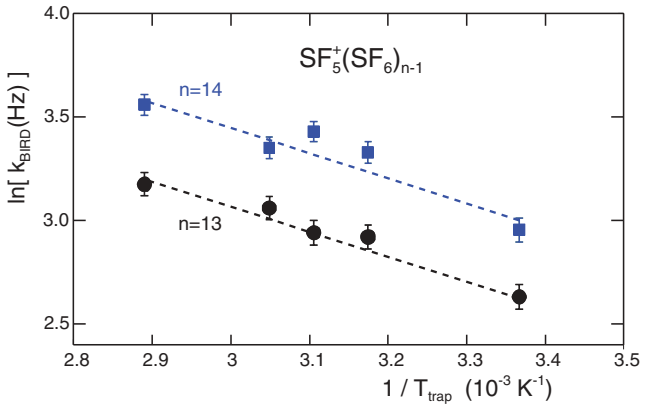

FIG. 5. (Color online) The BIRD rates k_{BIRD} as a function of trap temperature T_{trap}, measured for $SF_5{}^+(SF_6)_{n-1}$ clusters with $n = 13$ and 14. The dashed lines represent a simultaneous fit using Eq. (4).

decay rates, derived from k_s by correcting for $k_{rg}(p)$ and k_{rf}, are displayed in Fig. 5, where the natural logarithm of k_{BIRD} is plotted as a function of $1/T_{\mathrm{trap}}$. Even though the temperature increase had to be limited to 15%, a pronounced increase of the BIRD rate is observed.

Following Eq. (2), the trap temperature dependence of k_{BIRD} is given by the temperature dependence of k_{IR}, which in turn is governed by Planck's radiation law. Assuming the IR absorption to be dominated by a single transition of energy $\hbar\omega \gg k_B T_{\mathrm{trap}}$, as expected to be the case for SF_6-based clusters (see Secs. I A and III B), the temperature dependence should be approximately given by

$$k_{\mathrm{BIRD}}(T_{\mathrm{trap}}) \propto k_{\mathrm{IR}}(T_{\mathrm{trap}}) \propto \frac{1}{\exp(\hbar\omega/k_B T_{\mathrm{trap}}) - 1} \approx \exp(-\hbar\omega/k_B T_{\mathrm{trap}}). \quad (4)$$

Thus $\ln k_{\mathrm{BIRD}}$ should depend linearly on $1/T_{\mathrm{trap}}$ with a slope equal to $-\hbar\omega/k_B$, which is indeed found to be the case, as shown in Fig. 5. Fitting simultaneously the slope of both data sets, one obtains $\hbar\omega = (105 \pm 25)$ meV, in excellent agreement with the transition energy of 117 meV of the dominant 10.6-μm absorption band of SF_6.

Several conclusions can be drawn already at this stage of analysis: For storage times $\gtrsim$50 ms, the fragmentation of the $SF_5{}^+(SF_6)_{n-1}$ clusters is dominated by the BIRD process, and taking into account the particle losses due to residual gas and RF-induced processes, the time dependence of the number of surviving clusters $N_n(t)$ can be reasonably well described by a single exponential with a characteristic decay constant k_{BIRD}. The BIRD rate is observed to scale approximately with the number of SF_6 molecules in the cluster, and the energy intake is found to proceed mainly via the dominating IR absorption band of SF_6 at 10.6 μm. Moreover, viewed as a function of the cluster number n, k_{BIRD} shows pronounced and statistically relevant fluctuations around the average trend that can be attributed to deviations of the individual barrier heights E_b^n from an average value $\langle E_b \rangle$ of the cluster against dissociation. On the other hand, to understand also the fast component of $N_n(t)$ and, in particular, to deduce from the $N_n(t)$ curves the activation energies E_b^n, more detailed modeling of the dissociation process is needed.

B. Master equation description of the BIRD process

Our model calculations are based on the master equation approach, which has been used before to model the BIRD process (see, e.g., [27,28]). After leaving the ion source, the bunch of cluster ions can be considered as an ensemble of noninteracting particles. We can thus determine the time evolution of the individual members of the ensemble independently by solving a master equation $\dot{\mathbf{P}}(t) = \mathcal{M}\mathbf{P}(t)$, where $\mathbf{P}(t) = [P_0(t), \ldots, P_i(t), \ldots]$ describes the probability to find the cluster in a certain state i at time t, while the matrix $\mathcal{M} = \{k_{i,j}\}$ contains the rates connecting state i to j. The time evolution of the ensemble is then given by summing up the probabilities $\mathbf{P}(t)$ calculated for different initial conditions characterizing the ensemble at $t = 0$.

To be able to apply this approach, several assumptions and simplifications have to be made. One of the main simplifications concerns the interaction of the $SF_5{}^+(SF_6)_{n-1}$ clusters with the ambient radiation field. We assume that the IR absorption only proceeds via the two well-known absorption bands of the SF_6 molecules at 10.6 and 16 μm corresponding to $\sim$117 and $\sim$75 meV, respectively. The energy-integrated cross sections and the central positions of the two bands have been investigated for gaseous as well as solid SF_6 [29]. In solid SF_6 the two centroid energies are found to be only slightly shifted downwards by a few percent. Furthermore, the absorption cross section of the main 10.6-μm band was found to stay approximately constant, while the cross section of the 16-μm band is about a factor of 2 larger for solid than for gaseous SF_6. In this work we use the gas-phase values, noting that the results do not change much by using the solid-phase values, since the absorption rate is dominated by the 10.6-μm band. Together with the Planck distribution and a trap temperature of $T_{\mathrm{trap}} = 297$ K, we find the following values for the two molar absorption rates k_{IR} and the corresponding average energies $\hbar\omega$ per absorption:

$$k_{\mathrm{IR},1}(\hbar\omega_1 = 75\,\mathrm{meV}) = 0.16\,\mathrm{Hz}$$
$$k_{\mathrm{IR},2}(\hbar\omega_2 = 117\,\mathrm{meV}) = 1.16\,\mathrm{Hz}. \quad (5)$$

The dominance of the absorption through the 10.6-μm band is obvious. IR absorption cross sections for $SF_5{}^+$ are not known. However, in view of the smaller number of degrees of freedom of $SF_5{}^+$ as compared to SF_6, we expect the $SF_5{}^+$ absorption rates to be at least a factor of $q \sim 0.8$ smaller than those of SF_6. We will actually estimate q from the measured decay curves. The IR absorption rates for $SF_5{}^+(SF_6)_{n-1}$ clusters are thus determined by multiplying the molar rates given in Eq. (5) by $(n - 1 + q)$ with $0 \leqslant q \leqslant 0.8$. Spontaneous or induced IR emission from the excited SF_6 molecules is neglected, as we assume that the absorbed energy is immediately dumped into the internal cluster degrees of freedom.

The IR-induced absorption k_+ and spontaneous and induced emission rates k_- via the cluster degrees of freedom were estimated using the dipole sum rule for harmonic oscillators [30] together with the Debye energy of $\hbar\omega_D = 4.3$ meV deduced from the heat capacity of solid SF_6 at low temperatures [20]. This leads to molar rates of $k_+ \approx k_- \approx 0.12$ Hz; compared to the dominating heating via the SF_6 absorption bands and in view of the low transition energies, the energy input via the cluster degrees of freedom can be safely neglected.

The fragmentation of an $SF_5^+(SF_6)_{n-1}$ cluster is dominated by the emission of a neutral SF_6 molecule, while the emission of heavier SF_6 conglomerates is expected to be unlikely. Moreover, compared to the evaporation of a molecular cluster unit, the emission of a molecular fragment such as that of an F atom is expected to be negligible in view of the grossly different binding energies (0.25 eV as compared to >1 eV). Following Refs. [31,32], we describe the monomer fragmentation rate $k_f(\epsilon)$ of a cluster with total internal excitation energy ϵ by an Arrhenius law:

$$k_f(\epsilon) = \nu \exp\left(-\frac{E_b}{k_B T_{\rm eff}(\epsilon)}\right), \tag{6}$$

where ν is the frequency factor and E_b the barrier energy against fragmentation. The decay temperature $T_{\rm eff}(\epsilon)$ is given by $T_{\rm eff}(\epsilon) = T(\epsilon) - E_b/(2C(T))$, where $T(\epsilon)$ denotes the (microcanonical) temperature and $E_b/(2C(T))$ is the so-called finite heat bath correction [31]. As the SF_6 fragment is expected to carry away only $\sim k_B T_i$ of kinetic energy, the internal energy ϵ' of the resultant $SF_5^+(SF_6)_{n-2}$ will be approximately given by

$$\epsilon' = \epsilon - (E_b + \eta\,\epsilon/n + k_b T_i), \tag{7}$$

where η is the percentage of internal energy carried by the SF_6 internal degrees of freedom ($\eta \approx 0.2$ at $T_i = 140$ K [20]).

To calculate $\epsilon(T)$, as well as the inverse function $T(\epsilon)$, the heat capacity $C_n(T)$ of an $SF_5^+(SF_6)_{n-1}$ cluster is needed. We use the molar heat capacity measured for solid SF_6 [20] but neglect the solid-solid phase transition at $\sim$95 K, which is expected to be smeared out in small SF_6-based clusters. Using a convenient parametrization, we find

$$C_n(T) = (n-1)[a(1-\exp(-bT)) + cT^2]k_B, \tag{8}$$

with $a = 5.68$, $b = 0.04$ K^{-1}, $c = 1.4 \times 10^{-4}$ K^{-2}.

The frequency factor appearing in Eq. (6) should be of the order of the vibrational frequencies of the cluster, i.e., $\nu \sim \omega_D/2\pi \sim 10^{12}$ s^{-1}. Estimates of ν along the lines suggested in Ref. [33] using an extrapolation of the measured vapor pressure curve of bulk SF_6 [34] to the temperature range of interest results, e.g., in $\nu \sim 10^{14}$–10^{15} s^{-1}. We shall use $\nu = 10^{13}$ s^{-1} in our model calculations.

Using the transition rates defined above and including the rates due to residual gas and RF-induced losses, the transition matrix $\mathcal{M}$ can be set up and the fate of an isolated $SF_5^+(SF_6)_{n-1}$ cluster with an initial intrinsic energy ϵ_0 can be calculated as a function of time by solving the master equation. To perform this calculation we first construct for a given ϵ_0 the scheme of possible excitation energies in the parent and daughter clusters using the transition energies given by Eqs. (5) and (7) (see Fig. 6). The time derivative of the population probability of a state at energy ϵ is then given by the sum over all possible feeding and decay probabilities, which are indicated by arrows in Fig. 6. By solving this set of time-dependent coupled equations, we obtain the probability of a cluster with initial energy ϵ_0 to end up as a cluster with energy ϵ at time t. To describe the full cluster ensemble at time t, we finally have to integrate over the initial energies ϵ_0 by taking into account the population probability of the initial states.

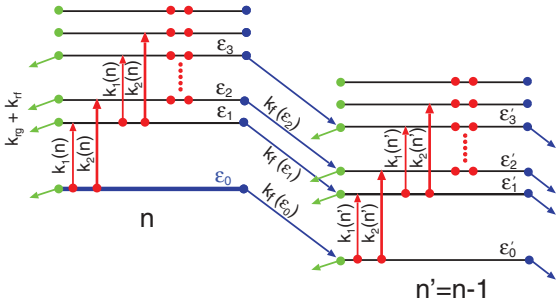

FIG. 6. (Color online) Schematic view of the time evolution of an isolated $SF_5^+(SF_6)_{n-1}$ cluster of size n and total initial energy ϵ_0. The IR absorption rates are given by $k_i(n) = (n - 1 + q)k_{{\rm IR},i}$, where $k_{{\rm IR},i}$ and the transition energies are tabulated in Eq. (5). The blue lines indicate the decay of the cluster by evaporation of an SF_6 monomer, while the green lines indicate the loss of a cluster due to residual gas collisions or RF-induced losses.

The calculation of the survival curve $N_n(t)$ of an ensemble of $SF_5^+(SF_6)_{n-1}$ clusters leaving the high-energy platform at time t_a is actually performed in two steps. In a first step, the internal excitation energy distribution $g_n(\epsilon)$ of the clusters at time t_a is calculated. Defining $P_{m,n}(\epsilon_0,\epsilon,t)$ as the probability of an $SF_5^+(SF_6)_{m-1}$ cluster with initial energy ϵ_0 to end up as an $SF_5^+(SF_6)_{n-1}$ cluster with energy ϵ at time t, $g_n(\epsilon)$ is given by

$$g_n(\epsilon) = \sum_{m \geqslant n} \int G_m(\epsilon_0) P_{m,n}(\epsilon_0,\epsilon,t_a) d\epsilon_0, \tag{9}$$

where the $P_{m,n}$ are determined by the master equation with the initial condition $P_{m,n}(\epsilon_0,\epsilon,t=0) = \delta_{m,n}\delta(\epsilon' - \epsilon_0)$, and $G_m(\epsilon_0)$ describes the initial internal excitation energy distribution of the ensemble of clusters at the moment they leave the formation zone and are becoming isolated ($t = 0$).

At time t_a, the clusters are accelerated to a common kinetic energy and their velocities are getting mass dependent. As a consequence, fragmentation products from decays occurring at times $t > t_a$ do not contribute to the Fourier signal used to deduce the survival probability of $SF_5^+(SF_6)_{n-1}$ clusters leaving the high-voltage platform (see Sec. II). For $t \geqslant t_a$, $N_n(t)$ can thus be calculated in a second step by

$$N_n(t) = \int g_n(\epsilon_0) \sum_{i \geqslant 0} P_{n,n}(\epsilon_0,\epsilon_i,t) d\epsilon_0, \tag{10}$$

where the $P_{n,n}$ are determined by solving the master equation with the initial condition $P_{n,n}(\epsilon_0,\epsilon_i,t = t_a) = \delta_{i,0}$.

To estimate $g_n(\epsilon)$ we assume that the initial excitation of the clusters after they get isolated from the formation zone can be described by an initial temperature T_i and approximate the initial energy distribution by [31]

$$G_n(\epsilon) = A(n)\frac{1}{\sqrt{2\pi\sigma^2}} \exp[-(\epsilon - \epsilon_T)^2/2\sigma^2], \tag{11}$$

with $\sigma^2 = k_B C_n(T_i) T_i^2$ and $\epsilon_T = \int_0^{T_i} C_n(T) dT$. The initial cluster abundance $A(n)$ is assumed to be a smooth function of the cluster number n, estimated from the time-of-flight spectrum observed with the pickup electrode of the trap in a single pass measurement (see also Sec. III D). We will refer to

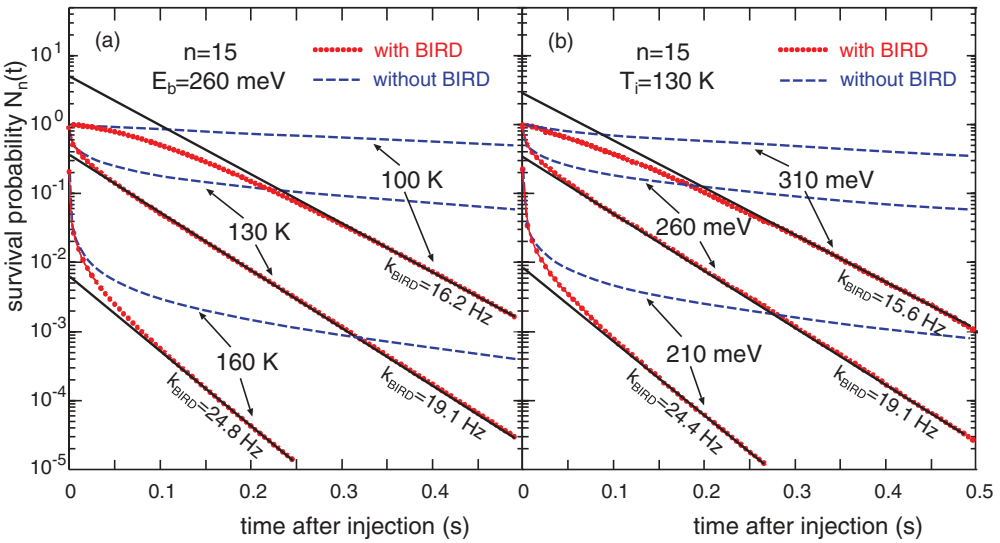

FIG. 7. (Color online) Model calculation of BIRD-induced decay curves for $SF_5^+(SF_6)_{n-1}$ clusters with $n = 15$, assuming (a) a barrier energy of $E_b = 260$ meV and three different initial temperatures T_i, and (b) an initial temperature of $T_i = 130$ K and three different barrier energies [dotted (red) lines]. The dashed (blue) lines show the corresponding curves if the BIRD effect is switched off. The solid (black) lines are fits of an exponential to the decay curves at long storage times, which result in the BIRD decay rates k_{BIRD}.

$G_n(\epsilon)$ as the source distribution. As the calculation of the time evolution of the cluster ensemble up to t_a requires knowledge of the barrier energies, we shall neglect this evolution in a first analysis step of the decay curves by assuming $t_a = 0$, i.e., setting $g_n(\epsilon) = G_n(\epsilon)$. The deduced barrier energies are then used in a second step to take into account that during the $t_a \sim 180\,\mu$s it takes to reach the acceleration zone, clusters with cluster number n are already decaying and are being formed due to the dissociation of heavier species.

To study the sensitivity of the decay curves to the initial temperature T_i and the barrier energy E_b, decay curves calculated (a) for a fixed barrier energy and three different initial temperatures and (b) for a fixed temperature and three different barrier energies are displayed in Figs. 7(a) and 7(b). Several conclusions can be drawn from this figure:

(i) The fast decrease of $N_n(t)$ at short storage times is caused by the dissociation of clusters with high initial internal energies. For lower initial temperatures [see Fig. 7(a)] the percentage of these clusters is smaller and for very low temperatures $N_n(t)$ is constant at early times—the clusters only fragment after enough IR photons are absorbed to overcome the activation barrier.

(ii) After approximately 30 ms the BIRD process starts to dominate the decay and the decay curves eventually become exponential with characteristic decay constants k_{BIRD}. Furthermore, for a given initial temperature T_i, k_{BIRD} is strongly correlated to the barrier energy E_b [Fig. 7(b)].

(iii) A comparison of the decay curves $N_n(t)$ calculated for $T_i = 160$ K, $E_b = 260$ meV, and $T_i = 130$ K, $E_b = 210$ meV reveals that they are very similar in shape; in fact, for the parameter space relevant in the present measurement, the survival probabilities are in first order only sensitive to the ratio E_b/T_i. A more detailed investigation of the decay curves is thus required to deduce independent information on the activation energy and the initial temperature.

Because of the complexity of the cluster formation process in a supersonic expansion ion source, there is no accepted procedure to estimate the internal energy distribution of the cluster after being isolated from the source. The approach taken in the present investigation is to assume that the initial internal energy distributions $G_n(\epsilon)$ of the clusters behind the Mach zone, where cooling collisions cease to take place, can be approximately described by a common temperature or by a temperature being at least a smooth function of the cluster number n. Another approach often used is that of an evaporative ensemble [35]. Here it is assumed that an ensemble of clusters with a broad internal energy distribution is leaving the collision zone and that each individual cluster is the product of at least one evaporation step. This leads to internal energy distributions $g_n(\epsilon)$ at time t_a when the acceleration takes place, which are limited on the low-energy side by ϵ_l fulfilling $k_f^{n+1}(\epsilon_l + E_b^{n+1})t_a \approx 1$ and on the high-energy side by ϵ_h fulfilling $k_f^n(\epsilon_h)t_a \approx 1$ as in the temperature approach.

In the evaporative ensemble approach, the $g_n(\epsilon)$ distributions are thus uniquely determined by the barrier energies E_b^n. It is therefore intriguing to use this prescription instead of the temperature approach to determine the barrier energies from the decay curves. It turns out, however, that it is not possible to obtain a self-consistent description of the data in this way. Starting, for example, from internal energy distributions $g_n(\epsilon)$ obtained by assuming a set of constant E_b^n—which look surprisingly similar to the distributions obtained when assuming a constant initial temperature—a modified set with on average larger barrier energies is obtained, which requires a new iteration with an effectively "hotter" energy distributions $g_n(\epsilon)$, and so on. No convergence can be reached. We attribute this failure of the evaporative ensemble approach to the underlying assumption that the internal energy of the clusters is only determined by the fragmentation process, therefore neglecting that clusters are also being cooled and thereby stabilized by collisions with the carrier gas of the supersonic expansion.

C. Barrier energies

Barrier energies were deduced from the decay curves $N_n(t)$ measured for $SF_5^+(SF_6)_{n-1}$ clusters with $n = 4$–28 in several steps using a χ-square fit routine: For a given initial temperature T_i, the decay curves were first fitted by varying E_b^n assuming $t_a = 0$ and restricting the fit to storage times >15 ms for reasons discussed in Sec. II. In the following steps t_a was set to 180 μs and the barrier energies from the last step were used to calculate the initial cluster population at t_a before performing a new fit of $N_n(t)$. After two iterations a stable set of barrier energies is obtained; the difference between the binding energies obtained in the first and final step is $\lesssim$4%. The procedure was then repeated for different initial temperatures and different values of the parameter q describing the IR absorption of SF_5^+.

Assuming the same initial temperature for all $SF_5^+(SF_6)_{n-1}$ clusters, the best overall description of the decay curves is obtained for $T_i = 140$ K and $q = 0.3$, as exemplified by the solid curves plotted in Fig. 3. The model reproduces reasonably well the loss of clusters observed at short storage times, which is due to the fragmentation of the internally most excited clusters of the stored ensemble before the BIRD process starts to dominate the time dependence of the cluster decay.

For storage times $t_e \gtrsim 50$ ms the model predicts an almost exponential decay, in approximate agreement with the experimental findings. For a more detailed discussion of the quality of the model fits in this time domain, we divide the decay curves by $N_{0,s}(n)\exp^{-k_s(n)t}$ deduced in the biexponential fit of the data described in Sec. III A. Examples of these reduced decay curves are shown for three characteristic cluster regions in Fig. 8; they clearly show small but statistically significant deviations from exponential behavior. For small clusters [Fig. 8(a)], these deviations are found to be mainly controlled by the parameter q describing the absorption of the SF_5^+ core, while for clusters around $n = 13$ [Fig. 8(b)] they are mainly controlled by the initial temperature T_i. This allows us to limit q and T_i to $q = 0.3 \pm 0.3$ and $T_i = (140 \pm 20)$ K. For heavier clusters [Fig. 8(c)], where the contribution of the SF_5^+ core to the BIRD-induced decays is becoming negligible, the decay curves are consistent with $T_i = 140$ K, although they are getting rapidly less sensitive to the initial temperature.

The barrier energies E_b resulting from the best overall fit of the decay curves obtained for $T_i = 140$ K and $q = 0.3$ are shown in Fig. 9. The error bars comprise only statistical errors,

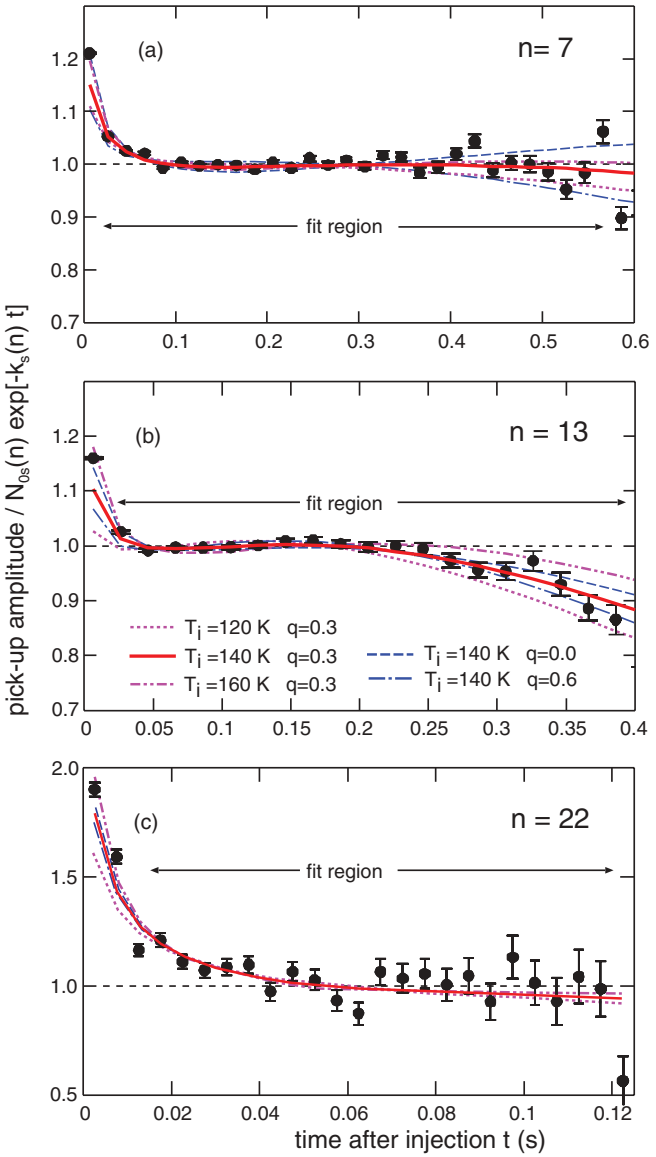

FIG. 8. (Color online) Reduced decay curves for $SF_5^+(SF_6)_{n-1}$ clusters with $n = 7$ (a), $n = 13$ (b), and $n = 22$ (c), which were obtained by dividing the measured curves by $N_{0,s}(n)\exp^{-k_s(n)t}$ deduced in the biexponential fit of the data described in Sec. III A. Also shown are the best fits obtained within the master equation approach by adjusting the barrier energies E_b^n and different assumptions concerning the initial temperature T_i and the relative contribution q of the SF_5^+ core to the BIRD process. In particular, the solid (red) curves represent the best overall ($4 \leqslant n \leqslant 28$) fit of the measured decay curves obtained for $T_i = 140$ K and $q = 0.3$.

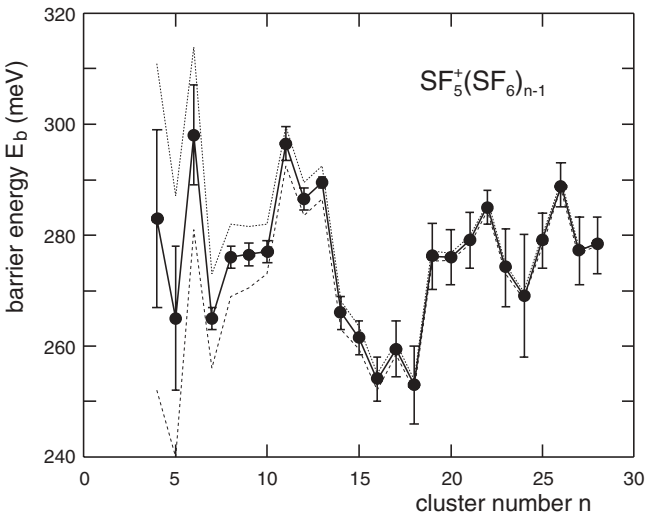

FIG. 9. Activation (barrier) energies of $SF_5^+(SF_6)_{n-1}$ clusters, deduced from the measured decay curves using the model description discussed in Sec. III B for an initial cluster temperature of $T_i = 140$ K and an SF_5^+ absorption parameter of $q = 0.3$. The error bars reflect statistical errors only, while the dashed (dotted) line corresponds to barrier energies assuming q to be 0 (0.6), respectively.

while the dashed (dotted) curve represents the resulting barrier energies by allowing q to vary within its uncertainty. The absolute scale of the barrier energies is mainly determined by the initial temperature T_i and the Arrhenius frequency factor ν; changing T_i by ± 20 K results in an overall shift of the barrier energies by ± 40 meV, and a change of ν within the limits $\nu = 10^{13\pm1}$ s^{-1} leads to a shift of ± 20 meV. We therefore estimate the absolute barrier energy scale to be accurate to within $\pm 25\%$. Relative barrier energies, on the other hand, are considered to be more precise, as we can expect the initial temperature to be—if not constant—at least a smooth function of the cluster size.

D. Source abundances

An additional input required in the model calculations concerns the initial source abundance $A(n)$. In the analysis presented so far, $A(n)$ was assumed to be a smooth function of n. As the deduced barrier energies turn out to be only marginally effected by the choice of the $A(n)$, we can use the results obtained in the previous section to approximately reconstruct the initial source abundance from the intensity pattern measured with the pickup mass spectrometry method. The validity of the procedure was then verified by using the reconstructed $A(n)$ in the analysis of the decay curves; the deduced barrier energies were found to stay well within the error bars.

The result of this reconstruction analysis is displayed in Fig. 10. The source abundances deduced from the mass spectrum can indeed be reasonably well approximated within their error bars by a smooth distribution with the exception of the statistically well-borne-out peak at $n = 13$, which was already reported by Echt *et al.* [17], and possibly of two additional structures at $n \approx 20$ and 25, whose statistical relevance, however, is smaller. The comparison between the source abundance and the intensity pattern of the mass spectrum, which is recorded by averaging over the first 80 ms of storage, clearly shows that the pronounced structure of the mass spectrum is caused by the BIRD-induced decays, i.e., by the stability of the clusters against fragmentation, and that the original source abundance, which is difficult to understand quantitatively, is only of minor importance. Note, however, that the dominance of the $n = 13$ peak in the mass spectrum is not only due to its enrichment in the source and its stability, but is also owed to the instability of the clusters with $n > 13$, which decay already during the drift to the acceleration gap and add to the relative $n = 13$ population.

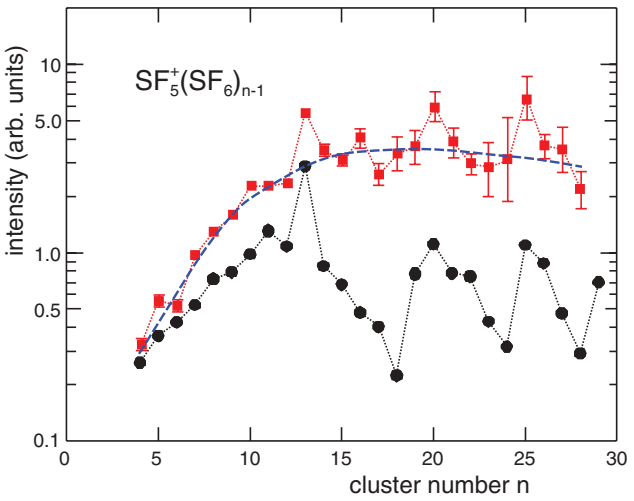

FIG. 10. (Color online) Relative intensity pattern of the stored $SF_5^+(SF_6)_{n-1}$ clusters, measured with the pickup mass spectrometry technique by averaging over the first 80 ms of storage [filled (black) circles]. The source abundances $A(n)$ reconstructed from these intensities are shown by the filled (red) squares, with error bars reflecting their uncertainties due to the statistical errors of the activation energies E_b. The dashed (blue) line is the smooth approximation of source abundances used in the analysis discussed in Sec. III C.

E. Results

It is worthwhile to ask whether one does gain additional insight into the structure and stability of clusters by measuring their BIRD rates, and by the detailed modeling presented here. While a master equation analysis of the decay curves is required to derive quantitative information about the stability of the $SF_5^+(SF_6)_{n-1}$ clusters, main structural aspects are already accessible via the BIRD lifetimes $\tau_{BIRD} = 1/k_{BIRD}$ or via the even less demanding measurement of the BIRD-enhanced intensity pattern using the pickup or kick-out mass spectrometry method. This is illustrated in Fig. 11, which compares the intensity pattern observed by averaging over the first 80 ms of storage to the (reduced) BIRD lifetimes

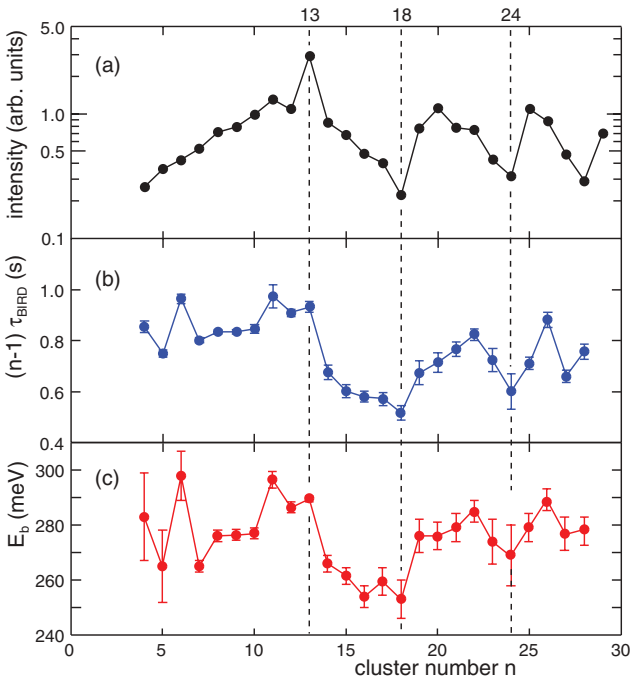

FIG. 11. (Color online) Results obtained from an increasingly more elaborated analysis of the BIRD-enhanced decays of $SF_5^+(SF_6)_{n-1}$ clusters with $n < 30$. (a) Intensity pattern measured with the pickup mass spectrometry method, averaging over 80 ms of storage. (b) Reduced BIRD lifetimes $(n-1)\tau_{BIRD}$ determined from the biexponential fit of the decay curves. (c) Barrier energies deduced using master equation modeling.

$(n-1)\tau_{\mathrm{BIRD}} = (n-1)/k_{\mathrm{BIRD}}$ deduced in Sec. III A and to the barrier energies E_b extracted in Sec. III B. As the mass spectrometry method is basically an integral measurement of the decay curves, there is a close correspondence between the structures in these graphs with peaks (valleys) in the BIRD-enhanced abundance spectrum reflecting long (short) BIRD lifetimes, which are correlated to barrier energies being larger (smaller) than the average.

One does, however, gain additional insight from measuring the BIRD rates [shown in Fig. 11(b)] even without detailed modeling. For instance, the BIRD rates indicate that the $n = 11$ cluster is more stable than the $n = 13$ cluster, and that the $n = 6$ cluster is especially stable. Both these features are not seen in the abundance spectra due to "pile-up" effects: clusters with $14 \leqslant n \leqslant 19$ are considerably less stable, causing them to emit SF_6 monomers until the more stable $n = 13$ is reached. Fragmentations such as these that occur before acceleration add to the increased abundance of $n = 13$. Such pile-up effects, however, are not expected to contribute considerably to the abundance of the $n = 6$ and $n = 11$ clusters since the slightly heavier clusters are in themselves relatively stable.

Thus a quantitative or even qualitative determination of the cluster binding energies from abundance measurements is very difficult and strongly hampered by the complexity of the production mechanism taking place in standard cluster sources. Alternative techniques are therefore required to determine these most fundamental properties of a cluster. The BIRD process is one of these methods, which can be applied to molecules and clusters of virtually any size. This is especially so within the rapid exchange limit, where the clusters' binding energies can be extracted directly by measuring the BIRD rate as a function of the trap temperature [see Eq. (1)]. The cationic SF_6 clusters investigated in the present study at room temperature fall into the slow exchange regime, which requires not only a detailed modeling of the absorption and dissociation process but also modeling of the initial internal excitation energy distributions in order to extract quantitative information about the cluster stability from the observed decay rates [9]. For SF_6-based clusters this modeling is considerably simplified, as the IR absorption, normally one of the greatest uncertainties in these calculations, is dominated by two well-known transitions bands of the SF_6 unit. Moreover, several other input parameters can be estimated from available detailed studies of bulk SF_6. The BIRD-enhanced decay observed when storing $SF_5{}^+(SF_6)_{n-1}$ clusters in a room-temperature trap therefore seemed to be well suited to determine the binding energies of an SF_6 unit in cationic SF_6-based clusters. Strictly speaking, the quantities deduced from BIRD measurements are the barrier energies E_b for the emission of an SF_6 unit, but as we expect the reverse association process of these weakly bound systems to be essentially barrierless, E_b can be set equal to the binding energy E_0 to a good approximation.

As it turns out, the barrier energies extracted from the decay curves using the master equation approach are strongly correlated to the initial internal energy distribution of the cluster, which we assume to be characterizable by a single parameter, the initial temperature T_i. Assuming an n-independent temperature, a global fit resulted in $T_i = (140 \pm 20)$ K and in barrier energies displayed in Fig. 9. An initial temperature of 140 K is reasonable for ionized clusters produced in supersonic expansion sources [4]. On the other hand, this temperature is only accurate to ± 20 K and is mainly determined by the fit of the lighter clusters with $n < 15$, which leaves room for a smooth dependence of the initial temperatures on n. In view of the strong correlation between initial internal energy distribution and barrier energy ($\Delta T_i = \pm 20$ K results in $\Delta E_b = \pm 40$ meV), not only the absolute scale but also the overall n dependence of E_b will change considerably when allowing T_i to vary within its error bars. Relative barrier energies between clusters being different by only a few cluster units, however, are considerably more accurate, and pronounced deviations from a smooth n dependence are observed, which indicates a subtle interplay between the forces acting between the cluster units and geometric considerations.

IV. THE STRUCTURE AND STABILITY OF $SF_5{}^+(SF_6)_{n-1}$ CLUSTERS

The structure and stability of $SF_5{}^+(SF_6)_{n-1}$ clusters is determined by the interplay of the monopole induced-dipole force between the molecular ion and the neutral units, the attractive van der Waals force between the constituents, and the interaction between the dipoles induced in the neutral molecules. Assuming the monopole induced-dipole force to be much stronger than the other two forces, we expect the monopole induced-dipole interaction to dominate the binding energy E_0 in small clusters while the other two interactions will only slightly decrease or increase E_0, depending on whether the van der Waals attraction or the dipole-dipole repulsion dominates. For this reason we expect the $SF_5{}^+$ unit to be located in the center of the cluster, thus minimizing the distance between it and the neutral units. The present measurements do not provide direct information concerning the position of the charged unit; however, we consider it likely that the clusters are in the thermodynamically most stable configuration at the beginning of the measurement. With increasing n, the role of the localized charge will become less important and we thus expect E_0 to decrease on average with increasing n until it reaches the bulk value of $\sim$230 meV at large n. This situation is different from that found for neutral clusters in which the forces between two cluster units can often be modeled using the Lennard-Jones potential; in this case the binding energies E_0 are expected to increase on average with increasing n before reaching the bulk value.

In view of the uncertainties of our data, it is unfortunately difficult to draw any solid conclusion concerning the average trend of the SF_6 binding energies at small n, but the small reaction enthalpies measured by Hiraoka *et al.* [19] of 202 and 150 meV for $n = 2$ and 3, respectively, can only be brought into accord with the present findings if the average binding energy is increasing with increasing n. This is rather counterintuitive; it would imply—as already suggested in Ref. [19]—an exceptionally weak monopole induced-dipole interaction between $SF_5{}^+$ and SF_6, comparable to the strength of the van der Waals attraction.

While the absolute binding energies determined in the present study are subject to large uncertainties, the binding energy differences observed between adjacent clusters are much more reliable. In particular, within the first shell, the $n = 6$ cluster is found to be exceptionally stable compared

to its neighbors (Fig. 11); its binding energy is more than 30 meV higher than observed for $n = 5$ and 7. Since the favorable position of an F atom of the neutral SF_6 units can be expected to be in between the fluoride atoms of the ionic core, and since there are five such positions, it is reasonable that the $SF_5{}^+(SF_6)_5$ cluster is especially stable. Moreover, the $n = 11$ cluster is observed to be more stable than the magic $n = 13$ cluster. Here a possible explanation may be that it is actually not even possible to fit the last two molecules around the central charged core without increasing the optimal distance of the already bound constituents from the center. (In an icosahedron, the distance between two neighboring vertices is smaller than the distance between every vertex and the center of the icosahedron.)

One of the most prominent and well-supported features of the data is the sharp drop of the barrier energies by ~30 meV after the closing of the first icosahedral shell at $n = 13$. This can be readily attributed to the fact that the additional molecules have to be placed for geometric reasons in the second shell, at roughly twice the distance from the core relative to the other molecules, and without stabilizing neighbors at least up to $n = 18$. The advantage of mass spectrometry relative to lifetime measurements is that it can be carried out also with low-intensity ion beams. While we have managed to measure the BIRD decay rates up to $n = 28$, using the mass spectrometry methods BIRD-enhanced abundances for the cationic $SF_5{}^+(SF_6)_{n-1}$ clusters could be determined up to $n = 100$. The results, obtained with the pickup as well as the kick-out technique, are shown in Fig. 12. The general trend exhibited by the data is an exponential decrease in cluster abundance as a function of cluster size, but on top of this distinct structures are visible: Between very pronounced "magic" peaks at $n = 13$,59, and 78, which signal very stable clusters considered to be due to geometrical shell closings,

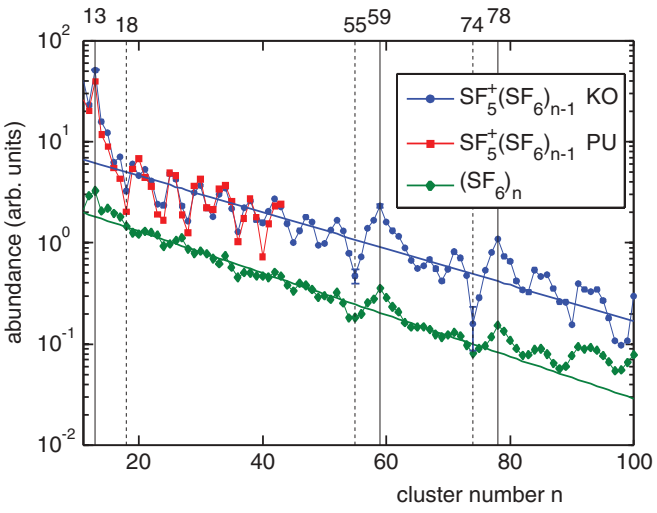

FIG. 12. (Color online) Comparison of the BIRD-enhanced abundances of cationic $SF_5{}^+(SF_6)_{n-1}$ clusters measured in the present study [kick-out mass spectrometry: filled (blue) circles; pickup mass spectrometry: filled (red) squares] with abundances observed by Ingolfsson and Wodtke [8] for anionic $(SF_6)_n{}^-$ clusters using electron attachment time-of-flight spectrometry [filled (green) diamonds]. Error bars are given for a few representative points.

a rich subshell structure is observed which involves weakly bound species, as indicated by the deep minimum occurring at $n = 18,24,28,32,36,40,45,49,55,\ldots$.

It is interesting to compare our results for cationic $SF_5{}^+(SF_6)_{n-1}$ clusters to those obtained for the anionic $(SF_6)_n{}^-$ species by Ingolfsson and Wodtke [8,13] using electron attachment time-of-flight spectrometry. The observed abundance pattern, which involves only short dwelling times, is plotted in Fig. 12 by the filled (green) diamonds. The anionic $(SF_6)_n{}^-$ abundances are commonly considered to represent the abundances of the neutral $(SF_6)_n$ species, as the electron attachment process is believed to proceed very gently, in particular when compared to the ionization-dissociation process connected with the production of cationic species [13]. However, the attachment energy of an electron to SF_6 is about 1 eV [36], which is dumped into the $SF_6{}^-$ breathing mode and subsequently into the intra- and intermolecular vibrations of the cluster. Electron attachment thus leads to an energy input into the cluster that is comparable to the total energy stored in an $(SF_6)_n$ for $n \sim 15$ at $T_i = 140$ K. The conjecture that the abundance pattern of $(SF_6)_n{}^-$ reflects that of the neutral species might therefore be limited to larger cluster sizes [8].

Remarkably, the abundance patterns of both cationic and anionic SF_6-based clusters display identical magic peaks also at $n = 59$ and 78. Even more, for clusters with $n \gtrsim 40$ also the subshell structures are observed to be identical for anionic and cationic clusters. We interpret this observation that for $n \gtrsim 40$ the influence of the charged cluster unit on the structure of the cluster is overwhelmed by the van der Waals interaction and that both cluster abundances reflect the structure and stability of the neutral $(SF_6)_n$ species. Thus both cluster series seem to confirm the conclusion of Refs. [8,13] that these aggregates are arranged in a monoclinic, bulklike, rather than in an icosahedral, packing. For $n < 40$, however, the subshell structure seems to be distinctly different for cationic and anionic SF_6 clusters, with the exception of the $n = 13$ cluster, which can be attributed to the first icosahedral shell closing, corresponding to a very compact and thus stable packing. The interpretation of the substructures in terms of geometrical subshells, as discussed for neutral species [8,13], remains open. Moreover, for a charge which is localized in one cluster unit, $SF_5{}^+$ or $SF_6{}^-$, one would expect the charge-induced interactions and their effect on the structure to be of similar size. It remains to be seen if the observed differences between cationic and anionic SF_6-based clusters are due to different charge distributions or due to the different symmetries and/or valencies of the charge carrier.

V. CONCLUSIONS

In the present work the stability of $SF_5{}^+(SF_6)_{n-1}$ clusters has been studied employing the blackbody-induced dissociation process. Using a supersonic expansion ion beam to produce the clusters and an electrostatic trap at room temperature to store them for up to 1 s, the survival probabilities of the clusters as a function of storage time were measured mass selectively. For storage times >30 ms, the cluster decay is found to be indeed dominated by the BIRD process and to exhibit an approximately exponential time dependence. The resulting characteristic decay constants k_{BIRD}

are observed to be on average proportional to the number of cluster units n, as expected for BIRD measurements within the slow exchange limit. The individual decay constants, however, show statistically relevant deviations from this average trend, which are indicative of an increased (decreased) stability of the cluster with respect to its neighbors. These stability-reflecting variations are also borne out in our mass spectrometry measurements. In contrast to usual abundance measurement, which involves dwelling times of at most a few 100 μs, the present mass spectrometric measurements involve an average over the first ~80 ms of storage and are thus strongly affected by the BIRD decay. These BIRD-enhanced abundance measurements lead to a markedly increased contrast as compared to usual abundance measurements, which are, in addition, mainly determined by the less-well-understood production probabilities of the clusters in the ion source.

While we could perform the BIRD-enhanced abundance measurements up to $n \sim 100$, the measurements of the individual decay curves had to be limited to $SF_5^+(SF_6)_{n-1}$ clusters with $n < 30$ due to intensity restrictions. When interested in major trends of the stability of clusters over a long cluster series, the mass spectroscopic measurements would thus be the method of choice. For a quantitative insight into the cluster stability, however, a more detailed analysis of the individual survival curves is required. We therefore used the master equation approach to describe the time dependence of the decay probability of an ensemble of $SF_5^+(SF_6)_{n-1}$ clusters with the aim of determining the binding energy of the least-bound SF_6 unit. While the description of the BIRD process is facilitated by the dominating and well-known absorption features of the SF_6 building blocks, the extraction of absolute binding energies is hampered by the strong correlation of the deduced binding energy to the initial temperature of the clusters, which both have to be determined from a fit of the decay curve. The best fits are obtained for initial cluster temperatures of ~140 K and result in binding energies between ~250 and ~300 meV for $SF_5^+(SF_6)_{n-1}$ clusters with $4 \geqslant n \geqslant 28$.

Although the uncertainty of the absolute binding energy scale is of the order of 25%, the analysis limits the absolute binding energies to values close to and consistent with the molar sublimation enthalpy of bulk SF_6 of ~230 meV. Moreover, the relative binding energies between neighboring clusters, which are expected to be considerably more reliable, reveal some interesting properties not seen in the mass spectrometry measurements, such as the extra stability of the $n = 6$ cluster and the larger binding energy of the $n = 11$ cluster as compared to that of the magic $n = 13$ cluster. Furthermore, by combining the individual binding energies together with the general trend observed in the BIRD-enhanced abundance measurements, a pronounced substructure in the stability of the cationic $SF_5^+(SF_6)_{n-1}$ clusters is observed between the magic cluster with $n = 13$,59, and 78. Abundance spectra measured by Ingolfsson and Wodtke [8] for anionic $(SF_6)_n^-$ clusters display the same magic numbers, and for $n > 40$ even the substructure pattern looks identical to that observed for the cationic species. This seems to indicate that for $n > 40$ the charge does no longer influence the structure of the SF_6-based cluster. For clusters with $n < 40$, however, the substructure is different for cationic and anionic species. While the magic numbers can be readily connected with the closure of geometric shells, the origin of the substructures and their different dependence on the charge of the cluster for $n < 40$ remains to be explained. We believe that the detailed results obtained in the present study establish the SF_6-based cluster as an interesting model system for studying the structural and energetic effects of a localized charge in ionic clusters.

ACKNOWLEDGMENTS

We thank A. M. Wodtke for supplying us with the data displayed in Fig. 12. We are grateful to R. D. Levine for his advice and helpful discussions. This research was supported by the Israeli Science Foundation (Grant No. 1242/09) and by the European Project ITS LEIF (Contract No. 026015). D. Schwalm acknowledges support by the Weizmann Institute of Science through the Joseph Meyerhoff program.

[1] W. D. Knight, K. Clemenger, W. A. deHeer, W. A. Saunders, M. Y. Chou, and M. L. Cohen, Phys. Rev. Lett. **52**, 2141 (1984).
[2] F. Naumkin and D. Wales, Mol. Phys. **93**, 633 (1988).
[3] G. Niedner-Schatteburg and V. E. Bondybey, Chem. Rev. **100**, 4059 (2000).
[4] H. Haberland, in *Clusters of Atoms and Molecules: Theory, Experiment, and Clusters of Atoms*, Springer Series in Chemical Physics (Springer, Berlin, 1994).
[5] H. W. Kroto, J. R. Heath, S. C. Obrien, R. F. Curl, and R. E. Smalley, Nature (London) **318**, 162 (1985).
[6] O. Echt, K. Sattler, and E. Recknagel, Phys. Rev. Lett. **47**, 1121 (1981).
[7] T. Martin, Phys. Rep. **273**, 199 (1996).
[8] O. Ingolfsson and A. M. Wodtke, J. Chem. Phys. **117**, 3721 (2002).
[9] R. C. Dunbar, Mass Spectrom. Rev. **23**, 127 (2004).
[10] U. Even, J. Jortner, D. Noy, N. Lavie, and C. Cossart-Magos, J. Chem. Phys. **112**, 8068 (2000).
[11] M. Dahan, R. Fishman, O. Heber, M. Rappaport, N. Altstein, D. Zajfman, and W. J. van der Zande, Rev. Sci. Instrum. **69**, 76 (1998).
[12] G. Herzberg, *Molecular Spectra and Molecular Structure II, Infrared and Raman Spectra of Polyatomic Molecules* (Van Nostrand, Princeton, NJ, 1968).
[13] O. Ingolfsson and A. M. Wodtke, Phys. Rev. Lett. **87**, 183401 (2001).
[14] G. Torchet, M. F. Deferaudy, and B. Raoult, J. Chem. Phys. **103**, 3074 (1995).
[15] A. Boutin, B. Rousseau, and A. H. Fuchs, Chem. Phys. Lett. **218**, 122 (1994).
[16] T. A. Beu, Y. Okada, and K. Takeuchi, Eur. Phys. J. D. **6**, 99 (1999).

[17] O. Echt, A. R. Flotte, M. Knapp, K. Sattler, and E. Recknagel, Ber. Bunsenges. Phys. Chem. **86**, 860 (1982).
[18] A. Stamatovic, P. Scheier, and T. D. Mark, J. Chem. Phys. **88**, 6884 (1988).
[19] K. Hiraoka, A. Shimizu, A. Minamitsu, M. Nasu, S. Fujimaki, and S. Yamabe, J. Am. Soc. Mass Spectrom. **6**, 1137 (1995).
[20] T. Ohta, O. Yamamuro, and H. Suga, J. Chem. Thermodyn. **26**, 319 (1994).
[21] W. D. Price, P. D. Schnier, and E. R. Williams, Anal. Chem. **68**, 859 (1996).
[22] H. B. Pedersen, D. Strasser, B. Amarant, O. Heber, M. L. Rappaport, and D. Zajfman, Phys. Rev. A **65**, 042704 (2002).
[23] D. Strasser, T. Geyer, H. Pedersen, O. Heber, B. Goldberg, S. Amarant, A. Diner, Y. Rudich, I. Sagi, M. L. Rappaport, D. J. Tannor *et al*., Phys. Rev. Lett. **89**, 283204 (2002).
[24] Y. Toker, N. Altstein, O. Aviv, M. L. Rappaport, O. Heber, D. Schwalm, D. Strasser, and D. Zajfman, J. Instrum. **4**, P09001 (2009).
[25] I. Rahinov, Y. Toker, O. Heber, D. Strasser, M. Rappaport, D. Schwalm, and D. Zajfman, Rev. Sci. Instrum. **83**, 033302 (2012).
[26] S. Menk (private communication).
[27] R. C. Dunbar, J. Phys. Chem. **98**, 8705 (1994).
[28] W. D. Price, P. D. Schnier, and E. R. Williams, J. Phys. Chem. B. **101**, 664 (1997).
[29] D. Dows and G. M. Wieder, Spectrochim. Acta **18**, 1567 (1962).
[30] J. U. Andersen and E. Bonderup, Eur. Phys. J. D **11**, 413 (2000).
[31] J. U. Andersen, E. Bonderup, and K. Hansen, J. Chem. Phys. **114**, 6518 (2001).
[32] J. U. Andersen, E. Bonderup, and K. Hansen, J. Phys. B **35**, 1R (2002).
[33] T. Schindler, C. Berg, G. Niedner-Schatteburg, and V. Bondybey, Chem. Phys. Lett. **250**, 301 (1996).
[34] http://encyclopedia.airliquide.com
[35] C. E. Klots, Z. Phys. D **5**, 83 (1987).
[36] A. A. Viggiano, T. M. Miller, J. Friedman, and J. Troe, J. Chem. Phys. **127**, 244305 (2007).